Quantum Cascade Laser-Based Measurement of Metal Alkylamide Density During Atomic Layer Deposition

JAMES E. MASLAR,* WILLIAM A. KIMES, and BRENT A. SPERLING

Material Measurement Laboratory, National Institute of Standards and Technology, 100 Bureau Drive, Stop 8320, Gaithersburg, Maryland 20899-8320

An in situ gas-phase diagnostic for the metal alkylamide compound tetrakis(ethylmethylamido) hafnium (TEMAH), $Hf[N(C_2H_5)(CH_3)]_4$, was demonstrated. This diagnostic is based on direct absorption measurement of TEMAH vapor using an external cavity quantum cascade laser emitting at 979 cm^{-1}, coinciding with the most intense TEMAH absorption in the mid-infrared spectral region, and employing 50 kHz amplitude modulation with synchronous detection. Measurements were performed in a single-pass configuration in a research-grade atomic layer deposition (ALD) chamber. To examine the detection limit of this technique for use as a TEMAH delivery monitor, this technique was demonstrated in the absence of any other deposition reactants or products, and to examine the selectivity of this technique in the presence of deposition products that potentially interfere with detection of TEMAH vapor, it was demonstrated during ALD of hafnium oxide using TEMAH and water. This technique successfully detected TEMAH at molecular densities present during simulated industrial ALD conditions. During hafnium oxide ALD using TEMAH and water, absorbance from gas-phase reaction products did not interfere with TEMAH measurements while absorption by reaction products deposited on the optical windows did interfere, although interfering absorption by deposited reaction products corresponded to only ≈4% of the total derived TEMAH density. With short measurement times and appropriate signal averaging, estimated TEMAH minimum detectable densities as low as ≈2×10^{12} molecules/cm^3 could be obtained. While this technique was demonstrated specifically for TEMAH delivery and hafnium oxide ALD using TEMAH and water, it should be readily applicable to other metal alkylamide compounds and associated metal oxide and nitride deposition chemistries, assuming similar metal alkylamide molar absorptivity and molecular density in the measurement chamber.

Index Headings: **Atomic layer deposition; ALD; Laser spectroscopy; Metal alkylamide; Infrared absorption; Quantum cascade laser; TEMAH; Tetrakis(ethylmethylamino) hafnium.**

INTRODUCTION

The development and demonstration of in situ gas-phase diagnostics for semiconductor manufacturing processes is potentially beneficial for a number of reasons. Such diagnostics can be utilized for advanced process control (APC) to enhance process productivity through, e.g., improved yields, reduced tool downtime, and reduced reactant waste.[1,2] In addition, gas-phase diagnostics can provide data for validation of equipment-scale process models. However, given the variety of processes and the necessary specificity of many diagnostics, there are a number of semiconductor processes for which in situ diagnostics have yet to be demonstrated. In fact, the "International Technology Roadmap for Semiconductors 2009 Edition" identifies sensor development as an important area for further research and development for both APC and model experimental validation.[1,3]

Atomic layer deposition (ALD) is a deposition process that is increasingly being utilized for depositing the nanometer-scale, conformal layers required for many microelectronics applications. In general, ALD is a deposition process in which material is deposited one monolayer (or sub-monolayer) at a time by sequentially exposing a chemically functionalized surface to reactive precursors.[4–6] A single deposition cycle consists of alternating injections of each reactive gas and an inert gas purge. A full deposition cycle involves injections of at least two different reactive gases. Deposition cycles are repeated until a target thickness is achieved. Microelectronics-related applications for ALD include the deposition of high permittivity (high κ) metal oxides for gate dielectrics in complementary metal oxide semiconductor (CMOS) technology and capacitor dielectrics in dynamic random access memory (DRAM) technology[4,5,7] as well as deposition of metal nitrides for diffusion barrier layers.[5,7,8] For the deposition of such materials, metal alkylamide compounds represent a technologically important class of metalorganic precursors, not only for ALD processes but also for chemical vapor deposition (CVD) processes.[4–14] These compounds are liquids or solids at room temperature and generally exhibit relatively low vapor pressures.[11,15,16] Therefore, it can potentially be difficult to reproducibly deliver these compounds from the source to the deposition surface.[17] Hence, pertaining to the development of processes involving metal alkylamides, an in situ technique that could help address potential delivery irreproducibility, e.g., by providing the basis for closed-loop delivery monitoring, would be particularly beneficial.

Optical diagnostics based on gas-phase infrared (IR) absorption spectroscopy have been demonstrated to be useful in probing aspects of various semiconductor manufacturing processes.[2,18] However, in the case of ALD processes, relatively few gas-phase IR absorption diagnostics have been demonstrated. Fourier transform infrared (FT-IR) spectroscopy has been used to observe both the reactants and products present during hafnium oxide ALD processes involving hafnium alkylamide compounds and water,[19–22] as well as platinum ALD involving a platinum cyclopentadienyl compound and molecular oxygen.[23] In addition, near-infrared (NIR) and mid-IR tunable diode laser-based systems have been used to monitor the ALD reactants water[19,24,25] and ammonia[25] under ALD gas-injection conditions. Also, a NIR laser-based system has been used to monitor the deposition product methane during aluminum oxide ALD from trimethylaluminum and water.[20,21] Hence, only Fourier transform infrared (FT-IR) spectroscopy has been demonstrated as a gas-phase diagnostic for metal alkylamide ALD. No laser-based measurements have been reported for metal alkylamide compounds: all of the species monitored during ALD with laser-

Received 13 September 2011; accepted 5 December 2011.
* Author to whom correspondence should be sent. E-mail: jmaslar@nist.gov.
DOI: 10.1366/11-06473

0003-7028/12/6603-0324$2.00/0
© 2012 Society for Applied Spectroscopy

based measurements have been relatively small molecules composed of only five atoms or less. This is unfortunate in that FT-IR spectroscopy suffers from somewhat limited temporal and spatial resolution under measurement conditions practical for an in situ diagnostic. In order to obtain better temporal and spatial resolution, laser-based absorption measurements are preferred.

The objective of this report is to describe the performance of an in situ gas-phase diagnostic for tetrakis(ethylmethylamido) hafnium (TEMAH), $Hf[N(C_2H_5)(CH_3)]_4$, a metal alkylamide that has been utilized in the CVD and ALD of hafnium oxide, hafnium silicate, and hafnium nitride.[10–14] This diagnostic is based on direct absorption measurement of TEMAH vapor using an external cavity quantum cascade laser (QCL) emitting at 979 cm^{-1}, coinciding with the most intense TEMAH absorption in the mid-infrared spectral region. To examine the detection limit of this technique for use as a TEMAH delivery monitor, this technique was demonstrated in a single-pass configuration in a research-grade ALD chamber in the absence of any other deposition reactants or products. To examine the selectivity of this technique in the presence of deposition products that potentially interfere with detection of TEMAH vapor, it was demonstrated during ALD of hafnium oxide using TEMAH and water. For this chemical system, only three gas-phase species are present during deposition in this reactor (based on in situ FT-IR spectroscopic measurements): the two reactants, TEMAH and water, and one secondary alkyl amine product, *N*-methylethanamine (MEA), $(CH_3)(C_2H_5)NH$, corresponding to the protonated ligand of TEMAH.[19,22] Hence, the only potential spectral interferences with TEMAH measurements are water and MEA, and water is injected at a different time than TEMAH. An additional objective of this work is to demonstrate the potential utility of this technique for use as a delivery monitor (in the absence of any other deposition co-reactants or products) or for use during ALD (in the presence of other co-reactants and/or products) for other metal alkylamide compounds besides TEMAH. The demonstration of this technique as a delivery monitor involves identifying the characteristic infrared vibrational frequencies of the tetrakis(dimethylamido) metal compounds, $M[N(CH_3)_2]_4$, the pentakis(dimethylamido) metal compounds, $M[N(CH_3)_2]_5$, the tetrakis(ethylmethylamido) metal compounds, $M[N(C_2H_5)(CH_3)]_4$, and the tetrakis(diethylamido) metal compounds, $M[N(C_2H_5)_2]_4$. The demonstration of this technique for use during ALD involves comparing the characteristic frequencies of the metal alkylamide compounds to the spectra of some potential co-reactants, H_2O, O_3, and NH_3, and to the expected corresponding secondary amine deposition products: *N*-methylmethanamine (MMA), $(CH_3)_2NH$, for the $M[N(CH_3)_2]_4$ and $M[N(CH_3)_2]_5$ compounds, MEA for the $M[N(C_2H_5)(CH_3)]_4$ compounds, and *N*-ethylethanamine (EEA), $(C_2H_5)_2NH$, for the $M[N(C_2H_5)_2]_4$ compounds.

EXPERIMENTAL PROCEDURE

Materials. Microelectronics-grade TEMAH (Air Products†) was purchased in a stainless-steel bubbler and employed as received without further purification to obtain a reference spectrum and to perform ALD. MEA (98+% purity, Alfa Aesar) and DEA (99.5% purity, Sigma-Aldrich) were received as liquids and anhydrous DMA (>99% purity, Sigma-Aldrich) was received as a liquefied gas. All three amines were utilized as received without further purification to obtain reference spectra. For delivery to the FT-IR spectrometer used for obtaining reference spectra, liquid MEA and DEA were transferred to a stainless steel vessel in a glove box under an inert atmosphere. DMA was delivered in the cylinder in which it was received using a gas regulator to control the delivery pressure. Deionized water with a resistivity of 18 MΩ·cm or greater at 21 °C was employed to perform ALD. Deposition was performed on 50 mm diameter (100) silicon wafers. Prior to deposition, wafers were dipped in a 2% HF solution for 30 s and then exposed to ozone for 4 min. Helium was purchased as an ultra-high-purity-grade gas (99.999% pure) and further purified with a bulk purifier.

Quantum Cascade Laser-Based Absorption Measurements. Figure 1 shows a schematic of the experimental configuration used to perform the QCL-based absorption measurements. The optical system will be described in this section while the ALD chamber and gas injection system will be described in the following section. A room-temperature, continuous-wave, external-cavity QCL (Daylight Solutions) was employed for the measurements described here. This QCL was capable of supplying greater than 10 mW of optical power at wavenumbers in the range of ≈925 cm^{-1} to ≈995 cm^{-1}, with a maximum of ≈60 mW at ≈955 cm^{-1}. For TEMAH absorption measurements, the laser system was tuned to 979 cm^{-1}, as measured with a mid-infrared laser wavelength meter. The QCL supplied ≈19 mW of optical power at 979 cm^{-1}. The laser output was amplitude modulated using a combination of two holographic wire grid polarizers fabricated on KRS-5 substrates, a ZnSe photoelastic modulator (PEM) operating at a nominal 50 kHz first-harmonic frequency (Hinds Instruments, Inc.), and a multi-order CdS quarter-wave plate with a nominal center wavelength of 10.2 μm (Gooch & Housego LLC). The optical axis of the first polarizer was oriented parallel to the direction of polarization of the laser radiation out of the laser head while the optical axis of the second polarizer was oriented perpendicular to that of the first polarizer. The optical axis of the PEM was oriented at 45 degrees with respect to the optical axis of the first polarizer. The optical axis of the quarter wave plate was parallel to that of the PEM. A PEM retardation of a 1/4-wave was employed, resulting in amplitude-modulated laser radiation with a nominal 50 kHz modulation frequency, an ideal maximum and minimum light intensity of 100% and 0%, respectively (assuming an ideal extinction ratio for the polarizers and zero absorption in the optical train), and a duty cycle of 50%.[26] To compensate for laser output intensity variations, the beam was divided into two beams of nominally equal power using a ZnSe beamsplitter that was coated for operation at a 45 degree angle of incidence and a wavelength of 10.6 μm. The reflected portion of the beam from the beamsplitter, referred to as the probe beam, was directed through the ALD chamber to a room-temperature, optically immersed (to a hyperhemispherical GaAs lens) photovoltaic multi-junction mercury cadmium zinc telluride detector with a 1 mm × 1 mm active area (VIGO System S.A.). The transmitted portion of the beam, referred to as the reference beam, was directed to a second nominally identical detector. The reported detectivity and responsivity of both detectors at

† Certain commercial equipment, instruments, and materials are identified in this publication to adequately specify the experimental procedure. Such identification in no way implies approval, recommendation, or endorsement by the National Institute of Standards and Technology, nor does it imply that the equipment, instruments, or materials identified are necessarily the best available for the purpose.

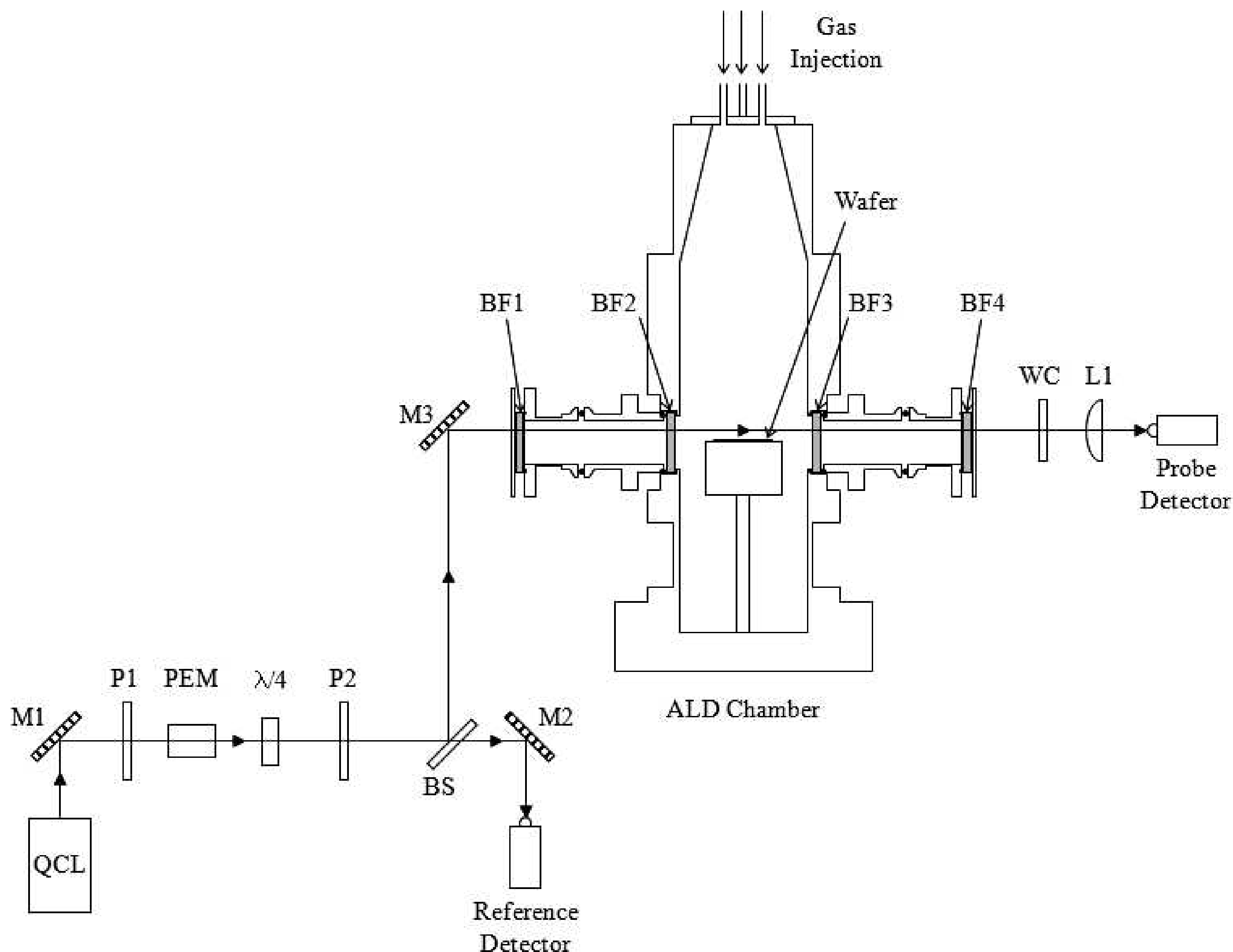

FIG. 1. Schematic diagram of the experimental configuration employed for the QCL-based measurements. QCL, quantum cascade laser; M1, M2, and M3, flat mirrors; P1 and P2, wire grid polarizers; PEM, photoelastic modulator; λ/4, quarter-wave plate; BS, beamsplitter; BF1, BF2, BF3, and BF4, barium fluoride windows; WC, wire cloth; L1, lens.

10.6 μm was $\approx 2 \times 10^8$ cm·Hz$^{1/2}$·W^{-1} and $\approx$2 V/W, respectively. The optical power on the detectors was kept below 0.5 mW to prevent saturation of the detectors. To achieve this power level on the probe beam detector, the probe beam was first attenuated with a 75 μm mesh (No. 200 alternative sieve designation) woven wire cloth and then focused onto the detector with a 38.1 mm focal length, 25.4 mm diameter plano-convex ZnSe lens with an anti-reflection coating optimized for 10.6 μm. All mirrors were protected gold flat mirrors. By moving the wafer chuck into and out of the beam and monitoring the probe detector power, the beam diameter in the region across the wafer was estimated to be $\approx$8.6 mm and the distance from the center of the beam to the wafer surface was estimated to be $\approx$9.6 mm (this was the only measurement position used for this report). The voltage output from each detector was amplified by a factor of 100 using a low-noise preamplifier. The output voltage from each preamplifier was filtered using a digital signal processing (DSP) lock-in amplifier. The 50 kHz PEM modulation frequency was used as the reference frequency, signal was detected at the reference frequency, and both lock-in amplifier time constants were 10 ms. The analog output of each lock-in amplifier was digitized at 200 Hz using an 18 bit data acquisition board. The start of a series of measurements (time zero) was synchronized with the start of a gas injection cycle. Data obtained from multiple injection cycles was averaged to improve the signal-to-noise ratio.

For the QCL-based absorption measurements, the Napierian absorbance, A_e, was calculated using the expression

$$A_e = -\ln\left(\frac{P_{probe}/P_{ref}}{P^0_{probe}/P^0_{ref}}\right) = -\ln\left(\frac{P_r}{P^0_r}\right) \quad (1)$$

where P_r is the ratio of the radiant power transmitted through the chamber incident on the probe detector (P_{probe}) to the radiant power incident on the reference detector at the corresponding time (P_{ref}) and P^0_r is the ratio of the radiant power transmitted through the chamber when TEMAH is nominally absent (P^0_{probe}) to the radiant power on the reference detector at the corresponding time (P^0_{ref}). For the TEMAH-only injection and ALD measurements, the P^0_r value was obtained

by taking the mean of 200 values of the ratio of the probe voltage to reference voltage corresponding to the time interval 0.5 s to 1.495 s during the initial 2 s helium purge. This time interval was selected since it was assumed to provide the most reproducible baseline absorption level. It was assumed that any potential gas flow perturbations due to valve switching would be minimized during this time interval. In addition, it was assumed that by this time the amount of residual TEMAH adsorbed to reactor surfaces would be minimized.

Atomic Layer Deposition System. Measurements were performed in a custom-designed and -built single-wafer, warm-wall, horizontal-flow deposition chamber with a pulsed gas injection system. Aspects of this deposition system have been described previously;[19,22] details pertinent to this investigation will be described here. Gases are injected from four ≈4.8 mm internal diameter (1/4″ outside diameter) electropolished stainless steel tubes into a conical section of the deposition chamber, the internal diameter of which expands to a ≈102 mm internal diameter cylindrical tube. The deposition chamber walls are aluminum up to 25.4 mm thick to facilitate uniform heating. A 50 mm diameter silicon wafer was mounted on a custom-designed wafer chuck such that the wafer surface normal is parallel to the direction of gas injection (the wafer surface normal is perpendicular to the table surface normal). The chuck was located in the center of the tube and consisted of an aluminum plate, to which the substrate was clamped, that was screwed to a stainless steel body, in which the heater was located. The distance from the gas injection port to the wafer surface was ≈253 mm. A mineral-insulated metal-sheathed type K thermocouple mounted into a thermocouple well in the stainless steel body was used to measure the temperature for active temperature control, while a nominally identical thermocouple was mounted in a thermocouple well in the aluminum plate (to which the substrate wafer was clamped) for the purpose of monitoring the substrate temperature. The standard uncertainty of a type K thermocouple is equal to 2.2 °C, $k = 2$, at 250 °C. For all measurements reported here, the TEMAH delivery lines were heated to ≈90 °C and all other delivery lines and the reactor walls were heated to ≈110 °C. The wafer chuck was not actively heated. In this mode of operation, both control and monitor thermocouples mounted in the wafer chuck reached ≈108 °C and, therefore, the corresponding wafer surface temperature was estimated to also be ≈108 °C.

For all TEMAH measurements described in this report, only two different gas injection sequences were utilized. One sequence involved injecting TEMAH with no other reactant gases and consisted of a 2 s helium purge (helium flowing through all four lines), a 3 s TEMAH injection (TEMAH and carrier gas flowing through one line and helium flowing through the other three), and an 8 s helium purge. This sequence will subsequently be referred to as TEMAH-only injection. The other sequence involved performing ALD and consisted of a 2 s helium purge, a 3 s TEMAH injection, a 9 s helium purge, a 0.1 s water injection (water flowing through one line and helium flowing through the other three), and a 15 s helium purge. This sequence will subsequently be referred to as ALD. During all measurements, the nominal flow rate at standard temperature and pressure (0 °C and 101.3 kPa) was 75 mL/min (sccm) through each line for a total nominal flow rate of 300 mL/min in the chamber. TEMAH vapor was delivered to the chamber using a helium carrier gas that was bubbled through the TEMAH bubbler that was heated to ≈75 °C, a temperature corresponding to a TEMAH equilibrium vapor pressure of ≈52 Pa (0.39 torr).[15,16] Water was injected at room temperature with no carrier gas. The amount of water injected was controlled with a needle valve down-stream of the water reservoir, which was adjusted so that the flow rate of water was approximately equal to a 75 mL/min flow rate of helium. All valves were fast-switching pneumatic diaphragm valves. The nominal chamber pressure was ≈133 Pa (1 torr) as measured with a capacitance manometer.

For optical access, 50 mm diameter, 4 mm thick BaF_2 windows with a 0.5 degree wedge (to reduce étaloning effects) were mounted on opposite sides of the reactor in window wells recessed into the reactor walls. The windows were sealed to the reactor using high-temperature perfluoroelastomer O-rings (Markez Z1216) that provided a clear aperture measuring ≈42 mm in diameter. The distance from the inside surface of the reactor wall to the window inside surface varied from ≈1.5 mm to ≈5 mm (assuming a 30% O-ring compression), due to the curvature of the reactor walls. The optical path length from window surface to window surface inside the reactor was nominally 107 mm (assuming a 30% O-ring compression or nominally 108 mm assuming no O-ring compression). This window configuration was employed to minimize perturbations to the gas flow and temperature profiles in the reactor, as verified with computational fluid dynamics simulations. When the reactor was heated with two windows in this recessed mounting configuration, probe beam intensity fluctuations increased compared to beam intensity fluctuations when the reactor was at room temperature (the magnitude of the reference beam intensity fluctuations did not change when the reactor was heated). The increase in probe beam intensity fluctuations upon heating the reactor walls to ≈110 °C from room temperature corresponded to an increase in the standard deviation of absorbance blank measurements (made in the absence of TEMAH) of up to 5 times, depending on the measurement conditions. The increased intensity fluctuation was attributed to beam steering resulting from turbulent density variations in the ambient gas around the windows. To minimize this effect and maximize the signal-to-noise ratio (S/N), the optical path on each side of the reactor was enclosed in a vacuum tube that was terminated on one end by one of the recessed BaF_2 windows in the reactor and on the other end by a nominally identical BaF_2 window. The inside surface of the second window was located ≈ 45.5 mm from the outside surface of the recessed window. Viton O-rings were used to make seals at each tube-to-window interface (i.e., each recessed reactor window had O-ring seals on both surfaces). The tube was evacuated to 2.66 Pa (≈0.02 torr), thereby lowering the gas density in this volume and minimizing beam steering, as well as localized convective cooling of the windows.

Measurement of Reference Spectra. The gas-phase absorption spectra of TEMAH, MEA, DMA, and DEA were recorded as a function of pressure in a custom-built optical cell in which the pressure was varied by filling with a vapor and evacuating with a molecular drag pump. Absorption spectra were measured using an FT-IR spectrometer equipped with a KBr beamsplitter and a liquid nitrogen cooled mercury cadmium telluride detector. The optical cell was located in the spectrometer sample compartment and configured for a single-pass transmission measurement. The optical cell had a

0.124 m path length, a ≈28 mL volume, and two KBr windows. The beam path between the FT-IR instrument module and the optical cell was enclosed with purge tubes, and the purge tubes and instrument module were purged with dry nitrogen for all measurements. All reference spectra were recorded with 1 cm^{-1} resolution and 128 scans were co-added. Pressure in the optical cell was measured with a capacitance manometer heated to ≈140 °C. The analyte vapor was directly introduced into the sample cell without the use of a carrier gas. For TEMAH injection, the TEMAH vessel was heated to ≈95 °C. For the TEMAH spectrum shown here, the nominal optical cell temperature and pressure were 100 °C and 31.5 Pa, respectively. MEA, DMA, and DEA vapors were delivered at room temperature. For the spectra shown here, the nominal optical cell temperature was 50 °C and the nominal cell pressures were 945 Pa, 960.7 Pa, and 931 Pa, for MEA, DMA, and DEA, respectively. The spectra measured using the FT-IR spectrometer at a particular cell pressure were converted to a nominal molar absorptivity, ε (m^2 mol^{-1}), from

$$\varepsilon = A_{10}/cl \qquad (2)$$

where A_{10} is the decadic absorbance, c is the mole concentration (mol m^{-3}), and l is the optical path length (m). A_{10} is calculated from $A_{10} = -\log_{10}(T)$ where T is the transmittance, which was taken to be the ratio of radiant power transmitted through the optical cell in the presence of an analyte vapor to the radiant power transmitted through the cell when the cell was evacuated.

RESULTS AND DISCUSSION

Wavenumber Selection for TEMAH Detection. It has been demonstrated that the only major gas-phase species present in this deposition chamber during ALD of HfO_2 using TEMAH and water are TEMAH, water, and MEA.[22] While the most intense modes in the TEMAH mid-IR spectrum are spectrally resolvable from those in the water spectrum, a number of TEMAH and MEA mid-IR modes are not resolved.[22] In addition, during ALD the number density of MEA was determined to be comparable to that of TEMAH at times near the beginning of the TEMAH injection (and then decays as reactive surface sites are consumed).[22] Hence, MEA represents a potential interference when attempting to detect TEMAH vapor. Figure 2 shows the molar absorptivity for TEMAH and MEA in the wavenumber range of (a) 500 cm^{-1} to 3500 cm^{-1} and (b) 750 cm^{-1} to 1250 cm^{-1}. As an aid to the eye, a vertical line is located at 979 cm^{-1}. The corresponding TEMAH absorbance spectrum is in agreement with previously reported spectra of TEMAH in the gas phase[19,22] and liquid phase.[27] The MEA absorbance spectrum is in agreement with the previously reported gas-phase MEA spectrum.[28] The most intense peak in the TEMAH spectrum is observed at 979 cm^{-1} and is attributed to a N–C stretching mode based on density functional theory quantum calculations.[19] At this wavenumber, the MEA absorbance is relatively low. The values of ε at 979 cm^{-1} are nominally 59 m^2/mol and 0.29 m^2/mol for TEMAH and MEA, respectively.

Measurements During TEMAH-Only Injection. Figure 3 shows the Napierian absorbance at 979 cm^{-1} as a function of time for one and the average of fifty TEMAH-only injection cycles (2 s helium purge, 3 s TEMAH, and 8 s helium purge). The times at which the valves on the TEMAH bubbler were opened and then closed are indicated by vertical lines at 2 s and 5 s, respectively. Based on the delay between when the TEMAH valve is opened and when the first TEMAH signal is observed, it takes about 150 ms for TEMAH to transit the distance from the bubbler valve to the measurement position at this flow rate. As expected, the scan corresponding to a single injection cycle exhibits a lower S/N than does the scan corresponding to the average of fifty cycles. The S/N for the single scan is ≈27 while that for the average of fifty cycles is ≈280.

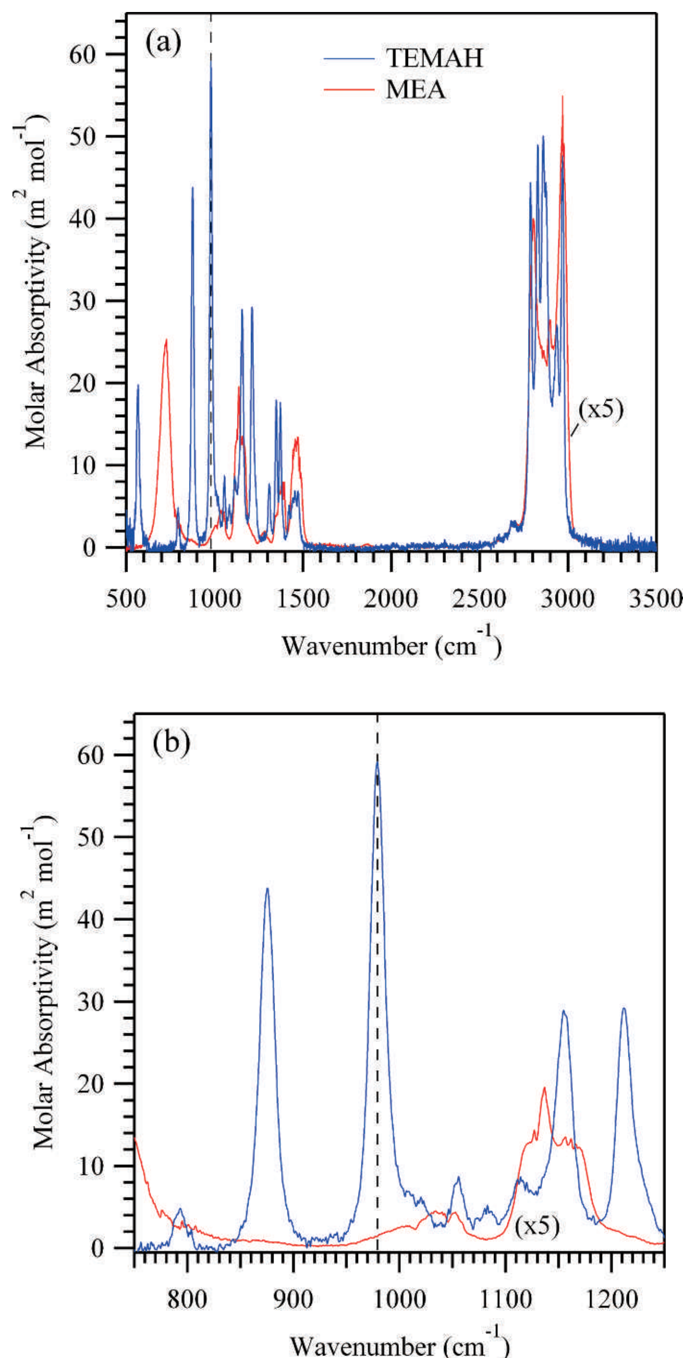

FIG. 2. The value of the molar absorptivity for TEMAH and MEA in the wavenumber range of (**a**) 500 cm^{-1} to 3500 cm^{-1} and (**b**) 750 cm^{-1} to 1250 cm^{-1}. The MEA molar absorptivity values are scaled by a factor of 5 for comparison. The vertical line is located at 979 cm^{-1}.

In an effort to further evaluate the practical performance

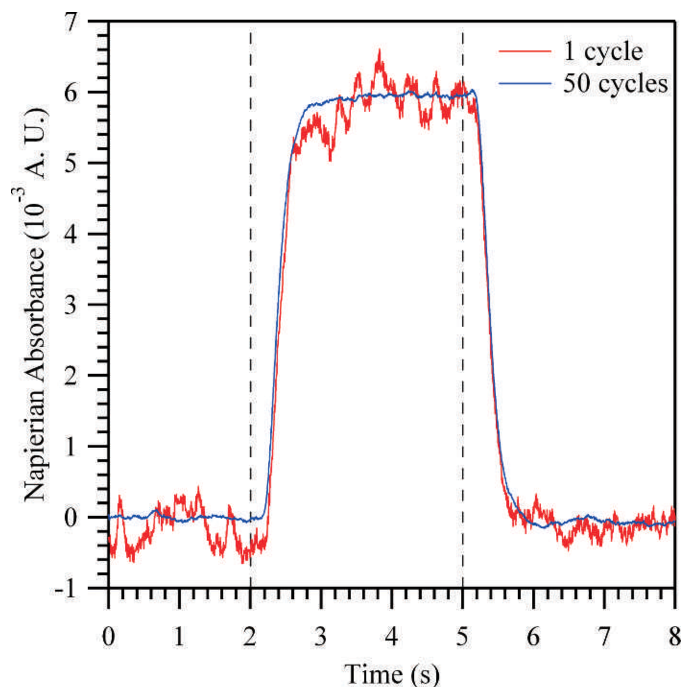

Fig. 3. The Naperian absorbance at 979 cm^{-1} as a function of time for one and the average of fifty TEMAH-only injection cycles. The vertical lines at 2 s and 5 s correspond to the opening and closing, respectively, of the values on the TEMAH bubbler.

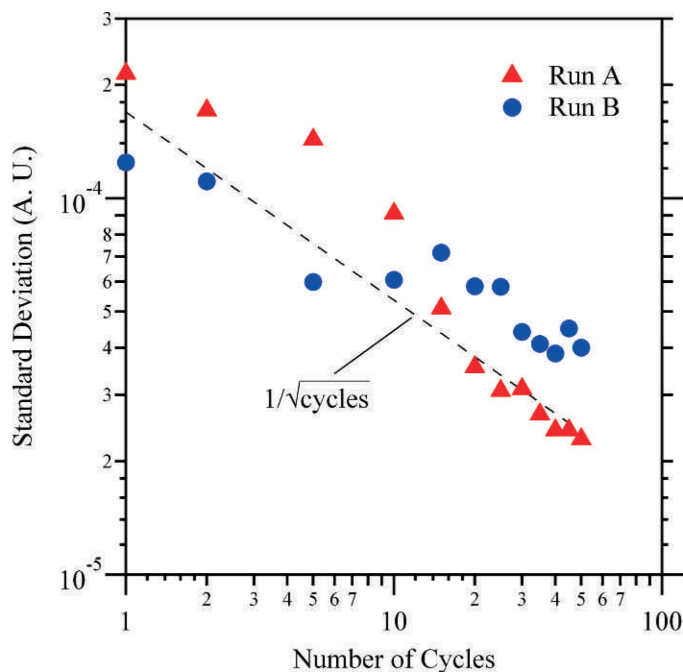

Fig. 4. The magnitude of the noise as characterized by the standard deviation of the absorbance during 1 s of inert gas purge before TEMAH injection. This value is obtained over a 1 s time interval for 1 injection cycle and for the average of 2, 5, 10, 15, 20, 25, 30, 35, 40, 45, and 50 TEMAH-only injections for two different runs of 50 TEMAH-only injections. The dashed line has a slope equal to the square root of the reciprocal of the number of injection cycles.

limits of this optical system, the standard deviation values of absorbance measurements made in the absence of TEMAH were determined under experimental conditions representing the two extremes of the presumed measurement conditions under which this technique would be employed: (1) relatively long measurement times with no signal averaging and (2) relatively short measurement times with signal averaging across multiple injection cycles. For the case of a long measurement time with no signal averaging, four consecutive 10 s helium purges were employed for a total time of 40 s. This time duration was selected because it exceeded the 30 s time interval over which the maximum laser intensity fluctuations of 2% to 3% tended to occur. For the case of a short measurement time with signal averaging, two TEMAH-only injections of 50 cycles each were employed.

For the 40 s helium purge, the absorbance was calculated using Eq. 1 with the blank absorbance measurement values (P_r^0) being calculated using the 200 voltage ratio values corresponding to the time interval 0.5 s to 1.495 s (as described previously). In this manner, a standard deviation of $\approx 1 \times 10^{-3}$ was calculated for the whole 40 s time interval.

For the TEMAH-only injections, the standard deviation was determined only from the 200 voltage ratio values corresponding to the time interval 0.5 s to 1.495 s. The standard deviation was calculated for 1 TEMAH-only injection cycle and for the average of 2, 5, 10, 15, 20, 25, 30, 35, 40, 45, and 50 injection cycles for two different runs of 50 injection cycles. These results are summarized in Fig. 4. In this figure, the observed values of the standard deviation varies from $\approx 2 \times 10^{-4}$ for a single injection cycle during Run A to $\approx 2 \times 10^{-5}$ for 50 injection cycles during Run A. The standard deviation values for Run B are also within this range. Also shown in Fig. 4 is a dashed line with a slope equal to the square root of the reciprocal of the number of injection cycles. The plots of the standard deviation value versus the number of injection cycles for Runs A and B both generally exhibit a slope equal to the reciprocal of the number of injection cycles. However, all of the points in these plots do not lie on the same line, suggesting a contribution from different noise sources over the course of these measurements.

It is difficult to definitively identify all of the major sources of noise in these measurements. However, one major source of noise was laser intensity instability. It was found that the laser intensity could vary as much 2% to 3% over a 30 s time interval, but not over every 30 s time interval. The relatively simple numerical ratiometric method employed here for intensity normalization was inadequate to completely compensate for these variations (possibly due to phase differences in the probe and reference detector channels). This effect likely contributes to the largest differences observed between Runs A and B in Fig. 4. There is also a somewhat periodic noise component observed in these data. This component can be seen in both traces in Fig. 3 (although it is difficult to see on the scale presented in Fig. 3 for the fifty cycle average trace) and exhibits a time interval that is generally in the 200 ms to 300 ms range. The origin of this component is unknown. It may be related to an étalon effect. (Étalon effects refer to the interference fringes due to the unintentional formation of a Fabry–Perot étalon involving any number of optical surfaces in this system.) If so, the frequency of this noise component suggests that it is more likely related to changes in étalon spacing due to mechanically induced drifts in the position of the optical components of this system rather than temperature-induced drifts. Another possible source of this periodic noise

component may be digital switching noise associated with the use of a DSP lock-in amplifier.[29]

As shown, the standard deviation values that are practically achievable with this experimental configuration are in the $\approx 1 \times 10^{-3}$ to $\approx 2 \times 10^{-5}$ range, depending on measurement time and number of cycles averaged. The minimum detectable quantity, q_L, of TEMAH was estimated for this range of standard deviation values using[30]

$$q_L = K s_{bl} / S \quad (3)$$

where s_{bl} is the standard deviation of the blank measurements, S is the sensitivity, and k is a numerical factor corresponding to the desired confidence level. Calculating the value of S from $S = \sigma_{net} l$, where σ_{net} is the net absorption cross-section given by $\sigma_{net} = 2.303\varepsilon / N_A$ with N_A being the Avagadro constant, and selecting $k = 3$, this range of s_{bl} values corresponds to q_L values of TEMAH from $\approx 1 \times 10^{14}$ cm^{-3} to $\approx 2 \times 10^{12}$ cm^{-3}.

Measurements During Atomic Layer Deposition. These q_L values of $\approx 1 \times 10^{14}$ cm^{-3} to $\approx 2 \times 10^{12}$ cm^{-3} were obtained during TEMAH-only injections and not under ALD conditions. Additional potential interferences exist for measurements performed during ALD that could limit the detectable TEMAH density. In particular, two potential interferences have been identified for HfO_2 ALD in this reactor using TEMAH and water: absorption by MEA generated from ALD on reactor and wafer surfaces and absorption due to reaction products on optical windows.[22] These two potential interferences were investigated by comparing number densities obtained during TEMAH-only injection and ALD measurements. Figure 5 shows the derived TEMAH number density as a function of time during TEMAH-only injection and ALD. The TEMAH-only (2 s helium purge, a 3 s TEMAH injection, and a 8 s helium purge) and ALD (2 s helium purge, a 3 s TEMAH injection, a 9 s helium purge, a 0.1 s water injection, and a 15 s helium purge) data represent the average of 25 cycles and 50 cycles, respectively. The times at which the valves on the TEMAH bubbler were opened and then closed are indicated by vertical lines at 2 s and 5 s, respectively, and the time the water valve was opened during the ALD cycles is indicated by the vertical line at 14 s. For both injection cycle types, the TEMAH number density increases from baseline to $\approx 2.5 \times 10^{14}$ cm^{-3}. In addition, TEMAH was first observed $\approx$325 ms later during ALD compared to TEMAH-only injection. This is attributed to the depletion of gas-phase TEMAH due to reactions of TEMAH with surface hydroxyl groups and/or adsorbed water on various chamber surfaces upstream of the measurement position and/or the wafer surface, the latter leading to depletion in the wafer surface boundary layer. (It is assumed that any residual water vapor levels will be the same during TEMAH-only and ALD gas injections and, therefore, any difference observed during TEMAH-only and ALD is due to TEMAH reaction with surface species). TEMAH depletion is not observed during TEMAH-only injection because after repeated TEMAH injections all surface sites are saturated and unreactive to TEMAH. The observation of this effect demonstrates that this gas-phase measurement can be used to estimate the necessary TEMAH injection time to saturate all reactive surface sites up-stream of the measurement position.

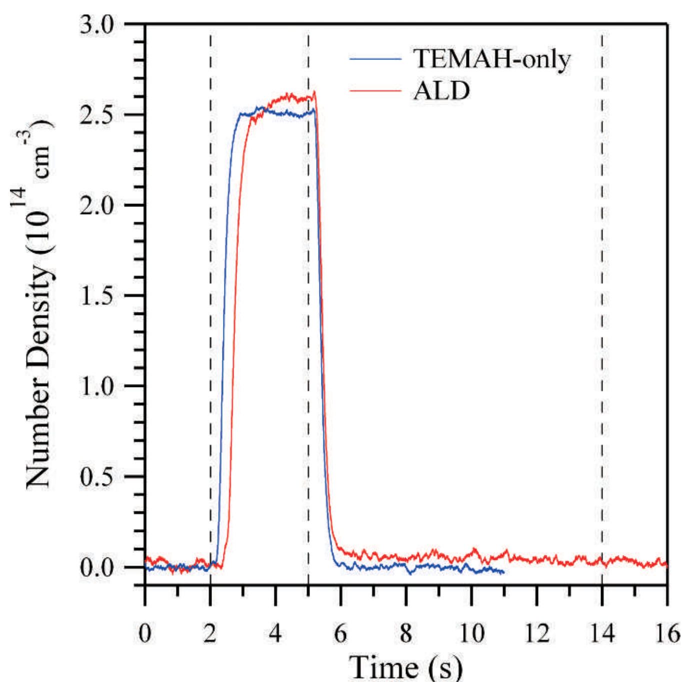

FIG. 5. The derived TEMAH number density as a function of time during TEMAH-only injection and ALD. The TEMAH-only and ALD data represent the average of 25 cycles and 50 cycles, respectively. The times at which the valves on the TEMAH bubbler were opened and then closed are indicated by vertical lines at 2 s and 5 s, respectively, and the time the water valve was opened during the ALD cycles is indicated by the vertical line at 14 s.

MEA absorption apparently does not interfere with TEMAH measurements at this wavenumber under these gas injection conditions. No increase in number density is observed in Fig. 5 during ALD for the water half cycle (starting at 14 s). This indicates that the molecular density of MEA produced during the water half cycle is below the detection limit. Assuming a value of $k = 3$, the minimum detectable quantity of MEA was estimated to be $\approx 5 \times 10^{14}$ cm^{-3} using Eq. 3 for $s_{bl} = 2 \times 10^{-5}$ and $\varepsilon = 0.29$ m^2/mol (assuming that the MEA ε value is independent of temperature from 50 °C to 110 °C). This MEA density is greater than the $\approx 4.5 \times 10^{14}$ cm^{-3} MEA number density that has been reported during the water half cycle for HfO_2 ALD in this reactor.[22] MEA is evolved during TEMAH injection by reaction of TEMAH with surface hydroxyl groups and residual water on the reactor surfaces and/or in the gas phase (the water having, e.g., desorbed from reactor surfaces and/or permeated through O-rings). However, the highest MEA density is observed during the water half cycle.[22] Hence, since no effect from MEA absorbance was observed during the water half cycle, it is concluded that the absorbance at 979 cm^{-1} during TEMAH injection is dominated by TEMAH absorbance.

Absorption due to reaction products on optical windows apparently was observed at 979 cm^{-1}. In Fig. 5, when TEMAH signal is observed during both TEMAH-only injection and ALD, the TEMAH number density is $\approx 1 \times 10^{13}$ cm^{-3} higher during ALD compared to TEMAH-only injection. Even after the TEMAH pulse is evacuated from the chamber at 6 s, it appears that the TEMAH number density is still $\approx 1 \times 10^{13}$ cm^{-3} higher during ALD compared to TEMAH-only injection. During HfO_2 ALD in this reactor, a surface-bound species containing TEMAH-like –N[$(C_2H_5)(CH_3)$] ligands (a species distinct from gas- or liquid-phase TEMAH) was observed on the optical windows.[22] Therefore, the $\approx 1 \times 10^{13}$ cm^{-3} difference in number density is attributed to the presence of

this species with an absorbance level of $\approx 2 \times 10^{-4}$ at 979 cm^{-1}. In addition, it appears that after water injection (at 14 s), the number densities during ALD and TEMAH-only injection both return to the baseline density, although this trend is difficult to definitively identify given the variations in absorbance observed for longer measurement times. If the higher number density observed during ALD is due to an adsorbed species, then presumably the return to baseline density after the water injection is due to the scrubbing by water of any remaining absorbed TEMAH-like species. Although the absorbing species may have similar ligands to MEA, the absorbing species is likely distinct from MEA for the reason given above (no change in number density was observed during water injection) and because little or no MEA density is observed after TEMAH has been exhausted,[22] which is in contrast to the $\approx 1 \times 10^{13}$ cm^{-3} difference in density which is observed for seconds after TEMAH is exhausted. While this density difference represents a measureable interference, under these conditions this interfering absorption corresponds to only $\approx 4\%$ of the total derived TEMAH density.

Application of this Technique to other Metal Alkylamide Compounds and Deposition Chemistries. While this technique was demonstrated specifically for TEMAH delivery and hafnium oxide ALD using TEMAH and water, it should be readily applicable to other metal alkylamide compounds for use as a delivery monitor (in the absence of any other deposition co-reactants or products) or for use during ALD (in the presence of other co-reactants and/or products), assuming similar metal alkylamide molar absorptivity and molecular density in the measurement chamber. For measurements during ALD in which deposition co-reactants and/or products are potentially present in the chamber, the utility of this technique is dependent on the specific process chemistry, although some generalizations can be made. Figure 6 shows (a) the characteristic frequencies for a number of metal alkylamide compounds; (b) the normalized line intensities of water, ozone, and ammonia (obtained from the HITRAN database[31]); and (c) the normalized molar absorptivity values for DMA, MEA, and DEA (obtained in this work) in the 800 cm^{-1} to 1400 cm^{-1} range. Figure 6a shows the characteristic frequencies for $M[N(CH_3)_2]_4$ (M = Ti, Zr, Hf) and $M[N(CH_3)_2]_5$ (M = Ta),[32–43] $M[N(C_2H_5)(CH_3)]_4$ (M = Ti, Zr, Hf),[22,27,44] and $M[N(C_2H_5)_2]_4$ (M = Ti, Zr, Hf).[32,39] Also shown in Fig. 6a is a box used to indicate the nominal wavenumber range of the QCL employed in this work. The co-reactants water, ozone, and ammonia were selected for comparison because these reactants are commonly utilized for oxide and nitride deposition.[6,10–14] DMA, MEA, and DEA were selected for comparison because one of these amines is the expected primary gas-phase thermal decomposition product for each of the metal alkylamide compounds shown in Fig. 6a.

Commercially available QCLs that operate at room temperature generally emit from ≈ 820 cm^{-1} to greater than 2300 cm^{-1}. A number of the metal alkylamide compounds exhibit multiple relatively intense absorption modes in the lower-wavenumber part of this range: absorptions are observed in the ≈ 871 cm^{-1} to ≈ 1371 cm^{-1} range for the compounds shown in Fig. 6a. Hence, QCL-based direct absorption measurements could be utilized as a delivery monitor for any number of metal alkylamide compounds. Furthermore, the exact experimental configuration described here could potentially be used for all of

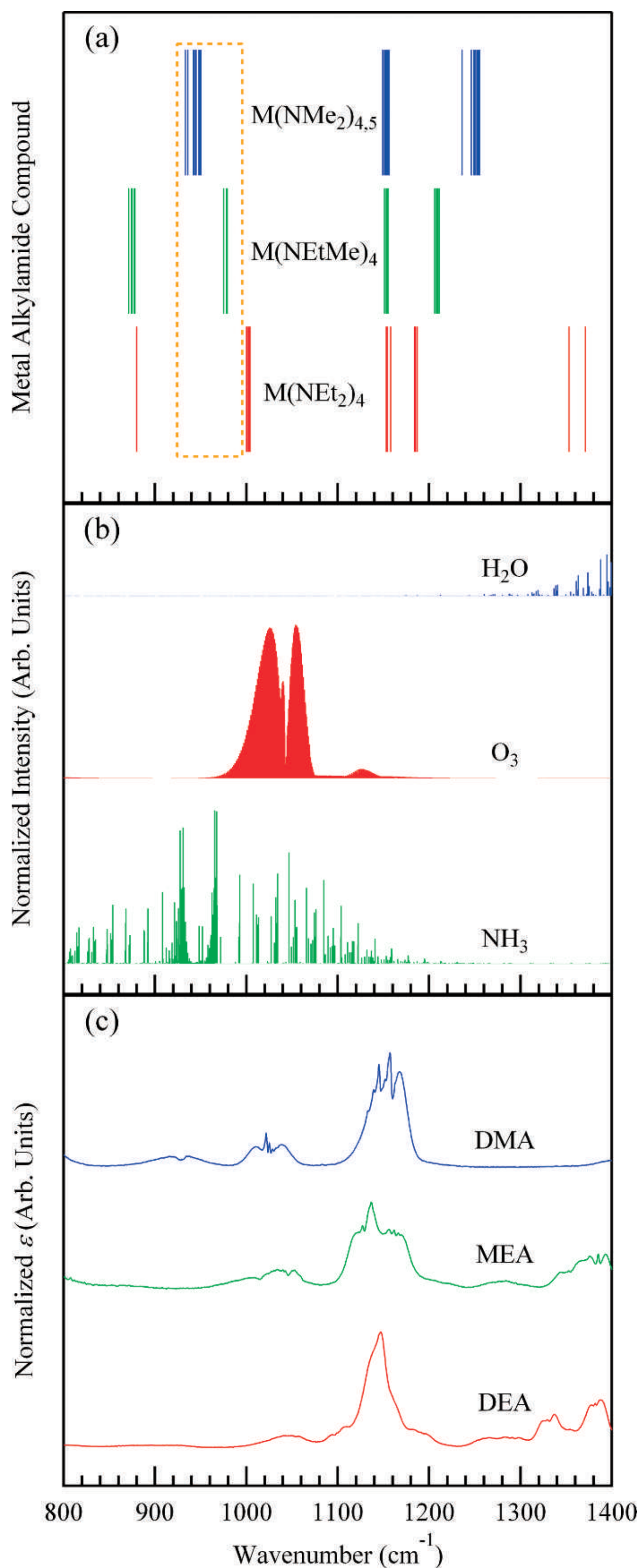

FIG. 6. (**a**) The characteristic frequencies for a number of metal alkylamide compounds; (**b**) the normalized line intensities of water, ozone, and ammonia (obtained from the HITRAN database[31]); and (**c**) the normalized molar absorptivity values for DMA, MEA, and DEA (obtained in this work) in the 800 cm^{-1} to 1400 cm^{-1} range. The box shown in (a) indicates the nominal wavenumber range of the QCL employed in this work.

the $M[N(CH_3)_2]_4$, $M[N(CH_3)_2]_5$, and $M[N(C_2H_5)(CH_3)]_4$ compounds shown in Fig. 6a.

The three co-reactants exhibit relatively intense, narrow absorptions throughout the $\approx$871 cm^{-1} to $\approx$1371 cm^{-1} range, as shown in Fig. 6b. However, there are a number of potential spectral windows, depending on the identity and density of the respective co-reactant. In addition, co-reactants are typically not present at the measurement point simultaneously during ALD, although this is not always the case. If co-reactants are temporally resolved, then interference with metal alkylamide absorption from co-reactant absorption is obviously not a problem. In fact, if the metal alkylamide and respective co-reactant are injected at different times, it may be possible to monitor both the metal alkylamide and a co-reactant with the same optical configuration. The three amine products exhibit relatively weak, broad absorptions throughout the $\approx$871 cm^{-1} to $\approx$1371 cm^{-1} range, as shown in Fig. 6c. Hence, depending on the metal alkylamide absorption being probed, it may be difficult to avoid interference from the amine product. However, it is possible that the absorbance associated with the amine is weak enough (e.g., due to a relatively low molar absorptivity) as to not significantly interfere with the metal alkylamide absorption measurement, as was demonstrated in this work to be the case for MEA and TEMAH.

CONCLUSION

An in situ gas-phase diagnostic for TEMAH was demonstrated. This diagnostic was based on a QCL emitting at 979 cm^{-1} and involved direct absorption measurements using 50 kHz amplitude modulation with synchronous detection. Measurements were performed in a single-pass configuration in a research-grade ALD chamber. To examine the detection limit of this technique for use as a TEMAH delivery monitor, this technique was demonstrated in the absence of any other deposition reactants or products, and to examine the selectivity of this technique in the presence of deposition products that potentially interfere with detection of TEMAH vapor, it was demonstrated during ALD of hafnium oxide using TEMAH and water. This technique successfully detected TEMAH at molecular densities present during simulated industrial ALD conditions. During hafnium oxide ALD using TEMAH and water, absorbance from gas-phase reaction products did not interfere with TEMAH measurements while absorption by reaction products deposited on the optical windows did interfere, although interfering absorption by deposited reaction products corresponded to only $\approx$4% of the total derived TEMAH density. Depending on the measurement time and degree of signal averaging, minimum TEMAH densities in the $\approx 1 \times 10^{14}$ cm^{-3} to $\approx 2 \times 10^{12}$ cm^{-3} range were obtained. While this technique was demonstrated specifically for TEMAH delivery and hafnium oxide ALD using TEMAH and water, it should be readily applicable to other metal alkylamide compounds and associated deposition chemistries.

ACKNOWLEDGMENTS

The authors gratefully acknowledge the NIST Office of Microelectronics Programs for funding, J. T. Hodges, W. S. Hurst, and S. Crivello for helpful discussions, P. M. Chu for assistance in obtaining the reference spectra, E. F. Moore for performing computational fluid dynamics simulations, and R. R. Fink for technical assistance in constructing the ALD chamber.

1. "Metrology", in The International Technology Roadmap for Semiconductors, 2009 Edition (2009), p. 29.
2. G. G. Barna and B. Van Eck, "In Situ Metrology," in *Handbook of Semiconductor Manufacturing Technology*, Y. Nishi and R. Doering, Eds. (Marcel Dekker, Inc., New York, NY, 2000), p. 797.
3. "Modeling and Simulation", in The International Technology Roadmap for Semiconductors, 2009 Edition (2009), p. 8.
4. J. Niinisto, K. Kukli, M. Heikkila, M. Ritala, and M. Leskela, Adv. Eng. Mater. **11,** 223 (2009).
5. M. Ritala and M. Leskela, "Atomic Layer Deposition," in *Handbook of Thin Film Materials*, H. S. Nalwa, Ed. (Academic Press, New York, 2002).
6. R. L. Puurunen, J. Appl. Phys. **97,** 121301 (2005).
7. M. Schumacher, P. K. Baumann, and T. Seidel, Chem. Vap. Deposition **12,** 99 (2006).
8. H. Kim, J. Vac. Sci. Technol., B **21,** 2231 (2003).
9. P. A. Williams, A. C. Jones, N. L. Tobin, P. R. Chalker, S. Taylor, P. A. Marshall, J. E. Bickley, L. M. Smith, H. O. Davies, and G. W. Critchlow, Chem. Vap. Deposition **9,** 309 (2003).
10. J. S. Becker, E. Kim, and R. G. Gordon, Chem. Mater. **16,** 3497 (2004).
11. D. M. Hausmann, E. Kim, J. Becker, and R. G. Gordon, Chem. Mater. **14,** 4350 (2002).
12. K. Kukli, M. Ritala, J. Lu, A. Harsta, and M. Leskela, J. Electrochem. Soc. **151,** F189 (2004).
13. K. Kukli, M. Ritala, T. Sajavaara, J. Keinonen, and M. Leskela, Chem. Vap. Deposition **8,** 199 (2002).
14. Y. Senzaki, S. Park, H. Chatham, L. Bartholomew, and W. Nieveen, J. Vac. Sci. Technol., A **22,** 1175 (2004).
15. H. Machida, T. Kada, M. Ishikawa, A. Ogura, and Y. Ohshita, Jpn. J. Appl. Phys., Part 1 **43,** 966 (2004).
16. S. A. Rushworth, L. M. Smith, A. J. Kingsley, R. Odedra, R. Nickson, and P. Hughes, Microelectron. Reliab. **45,** 1000 (2005).
17. W. L. Holstein, Chem. Eng. Sci. **49,** 2097 (1994).
18. I. P. Herman, "Section 8.2 Gas Phase Absorption," in *Optical Diagnostics for Thin Film Processing* (Academic Press, Inc., San Diego, CA, 1996), p. 272.
19. J. E. Maslar, W. S. Hurst, D. R. Burgess, W. A. Kimes, N. V. Nguyen, E. F. Moore, and J. T. Hodges, ECS Trans. **13,** 139 (2008).
20. A. O'Mahony, M. E. Pemble, and I. M. Povey, J. Mol. Struct. **976,** 324 (2010).
21. A. O'Mahony, I. M. Povey, and M. E. Pemble, ECS Trans. **16,** 349 (2008).
22. B. A. Sperling, W. A. Kimes, J. E. Maslar, and P. M. Chu, J. Vac. Sci. Technol., A **28,** 613 (2010).
23. W. M. M. Kessels, H. C. M. Knoops, S. A. F. Dielissen, A. J. M. Mackus, and M. C. M. van de Sanden, Appl. Phys. Lett. **95,** 013114 (2009).
24. R. Inman, A. Deshpande, D. Chraibi, and G. Jursich, "Atomic Layer Deposition of Hafnium Oxide Films Using Tetrakis Diethylamino Hafnium Precursor," in *SEMI Technology Symposium: Innovations in Semiconductor Manufacturing* (SEMI, San Jose, CA, 2003), p. 205.
25. M. Pemble, I. M. Povey, and F. Chalvet, ECS Trans. **11,** 155 (2007).
26. "Light Intensity Modulation Using a PEM", *Application Note* (Hinds Instruments, Inc., Portland, OR, 2010).
27. B. C. Kan, J. H. Boo, I. Lee, and F. Zaera, J. Phys. Chem. A **113,** 3946 (2009).
28. J. R. Durig, C. Zheng, W. A. Herrebout, and B. J. van der Veken, J. Mol. Struct. **641,** 207 (2002).
29. "Digital Noise at Lock-in Amplifier Input Connectors," *Technical Note TN 1008* (AMETEK Advanced Measurement Technology, Inc.: 2009).
30. IUPAC, Pure Appl. Chem. **45,** 99 (1976).
31. L. S. Rothman, I. E. Gordon, A. Barbe, D. C. Benner, P. E. Bernath, M. Birk, V. Boudon, L. R. Brown, A. Campargue, J. P. Champion, K. Chance, L. H. Coudert, V. Dana, V. M. Devi, S. Fally, J. M. Flaud, R. R. Gamache, A. Goldman, D. Jacquemart, I. Kleiner, N. Lacome, W. J. Lafferty, J. Y. Mandin, S. T. Massie, S. N. Mikhailenko, C. E. Miller, N. Moazzen-Ahmadi, O. V. Naumenko, A. V. Nikitin, J. Orphal, V. I. Perevalov, A. Perrin, A. Predoi-Cross, C. P. Rinsland, M. Rotger, M. Simeckova, M. A. H. Smith, K. Sung, S. A. Tashkun, J. Tennyson, R. A. Toth, A. C. Vandaele, and J. Vander Auwera, J. Quant. Spectrosc. Radiat. Transfer **110,** 533 (2009).
32. D. C. Bradley and M. H. Gitlitz, J. Chem. Soc. A, 980 (1969).
33. H. Bürger and W. Sawodny, Spectrochim. Acta, Part A **23,** 2841 (1967).
34. H. Bürger, H. Stammreich, and T. Teixeira Sans, Monatsh. Chem. **97,** 1276 (1966).
35. L. H. Dubois, B. R. Zegarski, and G. S. Girolami, J. Electrochem. Soc. **139,** 3603 (1992).
36. I. W. Kim, S. J. Kim, D. H. Kim, H. Woo, M. Y. Park, and S. W. Rhee, Korean J. Chem. Eng. **21,** 1256 (2004).
37. K. J. Li, S. G. Li, N. Li, D. A. Dixon, and T. M. Klein, J. Phys. Chem. C **114,** 14061 (2010).

38. J. C. F. Rodriguez-Reyes and A. V. Teplyakov, J. Phys. Chem. C **111,** 4800 (2007).
39. M. G. M. van der Vis, R. J. M. Konings, A. Oskam, and R. Walter, J. Mol. Struct. **323,** 93 (1994).
40. B. H. Weiller, J. Am. Chem. Soc. **118,** 4975 (1996).
41. J. Y. Yun, M. Y. Park, and S. W. Rhee, J. Electrochem. Soc. **145,** 2453 (1998).
42. J. Y. Yun, M. Y. Park, and S. W. Rhee, J. Electrochem. Soc. **146,** 1804 (1999).
43. J. Driessen, J. Schoonman, and K. F. Jensen, J. Electrochem. Soc. **148,** G178 (2001).
44. S. J. Kim, B. H. Kim, H. G. Woo, S. K. Kim, and D. H. Kim, Bull. Korean Chem. Soc. **27,** 219 (2006).